



Original articles

A mixed finite element method for nonlinear radiation–conduction equations in optically thick anisotropic media

Youssef Belhamadia^{a,*}, Mohammed Seaid^b^a American University of Sharjah, Department of Mathematics and Statistics, Sharjah, United Arab Emirates^b Department of Engineering, University of Durham, South Road, DH1 3LE, United Kingdom

Received 13 April 2023; received in revised form 11 July 2023; accepted 21 August 2023

Available online 9 September 2023

Abstract

We propose a new mixed finite element formulation for solving radiation–conduction heat transfer in optically thick anisotropic media. At this optical regime, the integro-differential equations for radiative transfer can be replaced by the simplified P_N approximations using an asymptotic analysis. The conductivity is assumed to be nonlinear depending on the temperature along with anisotropic absorption and scattering depending on both the direction and location variables. The simplified P_N approximations are enhanced by considering a diffusion tensor capable of describing anisotropic radiative heat transfer. In the present study, we investigate the performance of the unified and mixed formulations combining cubic P_3 , quadratic P_2 , and linear P_1 finite elements to approximate the temperature in the simplified P_3 model. To demonstrate the performance of the proposed methodology, three-dimensional examples of nonlinear radiation–conduction equations in optically thick anisotropic media are presented. The obtained numerical results demonstrate the accuracy and efficiency of the proposed mixed finite element formulation over the conventional unified finite element formulation to accurately solve the simplified P_3 equations in anisotropic media.

© 2023 The Author(s). Published by Elsevier B.V. on behalf of International Association for Mathematics and Computers in Simulation (IMACS). This is an open access article under the CC BY-NC-ND license (<http://creativecommons.org/licenses/by-nc-nd/4.0/>).

Keywords: Radiation–conduction heat transfer; Simplified P_N approximations; Mixed finite element methods; Three-dimensional optically thick media

1. Introduction

Modeling and simulation of radiative heat transfer is an important research area in all physical and engineering applications that involve high temperatures such as combustion chambers for gas turbines [15,34], powerful industrial furnaces [13,16], continuous casting [8,27,32], glass manufacturing [14,24] among others. In these applications, modeling heat transfer mainly involves conduction and radiation mechanisms as well as other processes including convection and chemical reactions. Conduction occurs in a relatively long time scale and transfers heat within the proximity of the heat source compared to radiation which transfers heat at the speed of light and it can affect objects far away from the heat source. At high temperatures, radiative transfer is also a key in these applications and it cannot be neglected in their modeling. For instance, experiments on semitransparent materials

* Corresponding author.

E-mail addresses: ybelhamadia@aus.edu (Y. Belhamadia), m.seaid@durham.ac.uk (M. Seaid).

have shown that the heat transfer cannot be estimated only by conduction but also by radiation. Indeed, in many annealing processes, the media temperature is higher than 1000 K and at this temperature, the radiation may dominate conduction. Mathematical modeling of radiative heat transfer in these applications requires solving integro-differential equations for the radiative transfer coupled to a set of parabolic-type partial differential equations for the thermal behavior of the medium, see [29,44] among others. However, solving these equations is not easy essentially because of the large set of dependent unknowns, the coupling between the radiation and the conduction, and the specular reflecting boundary conditions. Several numerical methods have been developed in the literature to overcome these difficulties including the zonal, Monte Carlo, and discrete ordinates methods. For more details on these methods, the reader is referred to [29,38,39,42] and further references are therein. However, these numerical methods still require high computational time and large memory storage particularly for radiative heat transfer problems in three space dimensions. Therefore, to produce large scale numerical simulations, fast and robust numerical solvers are needed to solve the radiation–conduction equations in optically thick anisotropic media.

During the last decade, research on radiative heat transfer has been shifted to the derivation of simple approximations which accurately predict the important physical phenomena at a reasonable computational cost. The most common approximate models are the simplified spherical harmonics method (also known by SP_N approximations) widely used when the medium is isotropic and optically thick, see for example [18,24–26]. Although these simplified approximations were derived using an asymptotic analysis for a large optical thickness of the medium, they still yield encouraging results in the optically thin regime. The SP_N approximations were first proposed in [25] and implemented in [24,26] for glass manufacturing, in [3] for crystal growth, in [15,38] for gas turbines, in [40,41] for flows at low Mach number, and in [1] for natural convection. Validation of results obtained using the SP_N approximations and experimental measurements has also been carried out in [36] for radiative transfer in combustion systems. Recently, comparison of SP_N approximations and the discrete ordinates method has been reported in [17] for radiative transfer in a turbulent jet flame. It should be stressed that the main advantage of the SP_N approximations is the use of a set of elliptic-type partial differential equations independent of the angular direction instead of the integro-differential radiative transfer equations. Furthermore, comparative results presented in the above-mentioned references have demonstrated that in optically thick media, the SP_N models approximate the full radiative heat transfer problem with an extremely low computational cost. However, only radiative heat transfer in isotropic media and with linear conductivity have been considered in these references. In many applications in thermal engineering at high temperatures, the conductivity becomes nonlinear depending on the temperature solution whereas the anisotropy in these applications is crucial. Our interest in the present study is on the SP_N approximations for nonlinear radiation–conduction problems in optically thick anisotropic media.

Numerical methods for solving the SP_N approximations have also attracted much research in the literature. For instance, a block Arnoldi method has been proposed in [43], continuous finite element methods have been implemented in [1,24], discontinuous finite element methods have been investigated in [19,21], enriched partition of unity finite element methods have been used to solve the SP_N models in [30,31], a static solution of the SP_3 approximation has been investigated in [28], and adaptive methods have been developed to accurately solve the SP_N models in [9,20,33]. For conduction–radiation problems with linear conductivity in isotropic media, these techniques have shown a significant gain in the computational time. However, they still require further study and improvements for nonlinear conduction–radiation problems in anisotropic media. It should also be noted that all the finite element methods for SP_N approximations employ the unified approach for which the same finite element spaces are used for the temperature and radiative solutions. For most applications for radiative heat transfer in optically thick media, the solution of interest is the temperature whereas the radiative solutions can be viewed as auxiliary variables in the problem under study. This would allow sacrificing some accuracy for the radiative solutions in the SP_N approximations while the temperature solution retains the higher accuracy. Thus, following similar ideas as those used for finite element methods for solving Navier–Stokes equations and Darcy problems, we propose a new mixed finite elements for solving the SP_N approximations. To our knowledge, mixed formulation where the temperature and radiative solutions are discretized in different finite element spaces has never been proposed in the literature.

In the present study, our proposed mixed finite element formulation for solving the SP_N models consists of using different spaces for the discretization of temperature and radiative solutions. Here, we implement the mixed $\mathbb{P}_m/\mathbb{P}_{m-1}$ finite elements for which the high-order elements \mathbb{P}_m are used for the temperature solution and the low-order elements \mathbb{P}_{m-1} are used for the radiative solutions. This results in a fast and accurate solver for nonlinear conduction–radiation problems in anisotropic media at optically thick regimes. Notice that the emphasis in the current work is on

the implementation of the proposed mixed finite element method for solving the SP_3 model but our method can be straightforwardly applied to other SP_N approximations without major conceptual modifications. To demonstrate our methodology, we consider the three-dimensional SP_3 equations where the conductivity is assumed to be nonlinear depending on the temperature describing anisotropic radiative heat transfer. In addition, the performance of the proposed mixed formulation is assessed using different discretizations combining the cubic \mathbb{P}_3 , quadratic \mathbb{P}_2 and linear \mathbb{P}_1 finite elements. To integrate the equations in time, we consider a fully implicit second-order Gear-based scheme and the Newton method is implemented to deal with the nonlinearity in the resulting system of equations. It should be pointed out that unlike the numerical methods in [1,24,30,31,40,41] where heat conduction and radiation equations are decoupled at each time step, the proposed mixed finite element method solves monolithically the fully coupled SP_3 equations. This provides an additional advantage related to the selection of timesteps in the simulations. Three numerical test examples for conduction–radiation problems, including a nonlinear problem in a three-dimensional anisotropic medium, are used to examine the performance of the proposed method. The mixed finite element method is assessed for various combinations of \mathbb{P}_1 , \mathbb{P}_2 , and \mathbb{P}_3 finite elements. The obtained results are also compared to those obtained using the unified finite element methods and against each others.

The rest of the paper is organized as follows. In Section 2 we introduce the nonlinear SP_3 approximation of the radiative heat transfer employed in this study. The formulation of the mixed finite element method for the SP_3 model is presented in Section 3. This section includes the time integration scheme and the different space discretizations used in the current study. Section 4 is devoted to numerical results using several three-dimensional test examples. Concluding remarks are summarized in Section 5.

2. Nonlinear SP_3 approximations of radiative heat transfer

In general, the radiation–conduction model consists of a heat conduction equation for the temperature $T(\mathbf{x}, t)$ coupled with an integro-differential equation for the radiative intensity $I(\mathbf{x}, s)$ at the point \mathbf{x} and with the propagation direction s , see for example [23,24,26,39,44]. In a dimensionless form, these equations read

$$\left\{ \begin{array}{ll} \frac{\partial T}{\partial t} - \nabla \cdot (\mathbf{K} \nabla T) = -\frac{1}{\tau^2} \nabla \cdot \mathbf{Q}, & (\mathbf{x}, t) \in \Omega \times [0, T_{final}], \\ \tau s \cdot \nabla I + (\kappa + \sigma)I = \frac{\sigma}{4\pi} \int_{\mathbb{S}^2} I(\mathbf{x}, s) ds + \kappa B(T), & (\mathbf{x}, s) \in \Omega \times \mathbb{S}^2, \\ \tau \mathbf{n}(\hat{\mathbf{x}}) \cdot \mathbf{K} \nabla T + h_c(T - T_b) = \alpha \pi (B(T_b) - B(T)), & (\hat{\mathbf{x}}, t) \in \partial\Omega \times [0, T_{final}], \\ I(\hat{\mathbf{x}}, s) = B(T_b), & (\hat{\mathbf{x}}, s) \in \partial\Omega^- \times \mathbb{S}^2, \\ T(\mathbf{x}, 0) = T_0(\mathbf{x}), & \mathbf{x} \in \Omega, \end{array} \right. \quad (1)$$

where $\Omega \subset \mathbb{R}^3$ is a bounded domain of an absorbing and emitting material with $\partial\Omega$ being its boundary and $[0, T_{final}]$ is the time interval. The parameters σ , κ , h_c and \mathbf{K} are the scattering coefficient, the absorption coefficient, the convective heat transfer coefficient and the thermal conductivity, respectively. In (1), \mathbb{S}^2 denotes the unit sphere, $\mathbf{n}(\hat{\mathbf{x}})$ the outward normal at $\hat{\mathbf{x}}$ to the boundary $\partial\Omega$, α the mean hemispheric surface emissivity, τ is a diffusion scale, and T_b a given ambient temperature of the surrounding. Here, $\nabla \cdot \mathbf{Q}$ denotes the radiative source term which can be calculated by the radiative information from the radiative transfer equation as

$$\nabla \cdot \mathbf{Q} = \kappa \left(4\pi B(T) - \int_{\mathbb{S}^2} I(\mathbf{x}, s) ds \right), \quad (2)$$

with $B(T)$ being the spectral intensity of the black-body radiation defined as

$$B(T) = \sigma_R T^4, \quad (3)$$

where $\sigma_R = 5.67 \times 10^{-8}$ is the Stefan–Boltzmann constant, see for instance [29]. Note that on the boundary we consider the transmitting conditions where the boundary region $\partial\Omega^-$ in (1) is defined as

$$\partial\Omega^- = \left\{ \hat{\mathbf{x}} \in \partial\Omega : \mathbf{n}(\hat{\mathbf{x}}) \cdot s < 0 \right\}.$$

It should be noted that Eqs. (1) have been widely used in the literature for modeling radiative heat transfer problems in participating media, see for example [26,29] and further references are therein. Numerical solutions of the radiative heat transfer Eqs. (1) have also been investigated and they cover statistical algorithms [29],

Table 1
Parameters and their values used in the SP₃ model.

Parameter	Value	Parameter	Value
α_1	2.3984	α_2	1.1432
β_1	0.0471	β_2	0.1612
η_1	32.1656	η_2	14.9583
μ_1	0.5888	μ_2	1.4915
γ_1	-16.221	γ_2	3.0617

raytracing techniques [23], direct S_n discrete-ordinates [22], and iterative solvers [38] among others. However, the main drawbacks of these methods are related to high computational costs and dense storage requirements in their implementations, see for example the comparative study reported in [15]. Furthermore, the radiative transfer equation in (1) is in a non-differential form, which presents a significant inconvenience when they are solved in conjunction with the differential equations governing the heat conduction, flow and combustion. One way to avoid these difficulties is to use the SP_N approximations for the radiative heat transfer Eqs. (1). These simplified equations are derived using an asymptotic analysis and they show excellent performance when the medium under consideration is optically thick (opaque), see for instance [24,26]. In the present study, we propose a mixed finite element method for solving the SP₃ model for anisotropic media but its application to SP₂ and SP₁ models can be carried out using the same manner. Hence, for heterogeneous and anisotropic media, the SP₃ equations are defined as

$$\left\{ \begin{array}{ll} \frac{\partial T}{\partial t} - \nabla \cdot (\mathbf{K} \nabla T) = -\frac{\kappa}{\tau^2} \left(4\pi B(T) - \frac{\gamma_2 \psi_1 - \gamma_1 \psi_2}{\gamma_2 - \gamma_1} \right), & (\mathbf{x}, t) \in \Omega \times [0, T_{final}], \\ -\tau^2 \mu_1^2 \nabla \cdot (\mathcal{E} \nabla \psi_1) + \kappa \psi_1 = 4\pi \kappa B(T), & (\mathbf{x}, t) \in \Omega \times [0, T_{final}], \\ -\tau^2 \mu_2^2 \nabla \cdot (\mathcal{E} \nabla \psi_2) + \kappa \psi_2 = 4\pi \kappa B(T), & (\mathbf{x}, t) \in \Omega \times [0, T_{final}], \\ \tau \mathbf{K} \nabla T \cdot \mathbf{n}(\hat{\mathbf{x}}) + h_c(T - T_b) = \alpha \pi (B(T_b) - B(T)), & (\hat{\mathbf{x}}, t) \in \partial \Omega \times [0, T_{final}], \\ \tau^2 \mu_1^2 \mathcal{E} \nabla \psi_1 \cdot \mathbf{n}(\hat{\mathbf{x}}) + \frac{\tau \mu_1^2 \alpha_1}{3} \psi_1 = -\frac{\tau \mu_1^2 \beta_2}{3} \psi_2 + \frac{\tau \mu_1^2 \eta_1}{3} B(T_b), & (\hat{\mathbf{x}}, t) \in \partial \Omega \times [0, T_{final}], \\ \tau^2 \mu_2^2 \mathcal{E} \nabla \psi_2 \cdot \mathbf{n}(\hat{\mathbf{x}}) + \frac{\tau \mu_2^2 \alpha_2}{3} \psi_2 = -\frac{\tau \mu_2^2 \beta_1}{3} \psi_1 + \frac{\tau \mu_2^2 \eta_2}{3} B(T_b), & (\hat{\mathbf{x}}, t) \in \partial \Omega \times [0, T_{final}], \\ T(\mathbf{x}, 0) = T_0(\mathbf{x}), & \mathbf{x} \in \Omega, \end{array} \right. \tag{4}$$

where the parameters $\alpha_i, \beta_i, \eta_i, \mu_i,$ and γ_i ($i = 1, 2$) are derived using a variational analysis as detailed in [26] and for completeness their values are listed in Table 1. Note that the SP₃ Eqs. (4) form a set of coupled elliptic- and parabolic-type equations and do not depend on the angle direction. These properties render the SP₃ (4) model more cost effective than the full radiative heat transfer model (1). It should also be stressed that most of studies reported in the literature for solving the SP₃ equations are only limited to linear problems with isotropic thermal and optical coefficients. In the current work, the interest is on heterogeneous anisotropic media for which the conductivity, absorption and scattering coefficients depend on the spatial location \mathbf{x} and the direction θ as well. In addition, the thermal conductivity may also depends on the temperature in a nonlinear manner and in this case the tensors \mathbf{K} and \mathcal{E} are defined by

$$\mathbf{K} = \mathcal{R}(\theta) \begin{pmatrix} K_{11}(T) & 0 & 0 \\ 0 & K_{22}(T) & 0 \\ 0 & 0 & K_{11}(T) \end{pmatrix} \mathcal{R}^{-1}(\theta),$$

$$\mathcal{E} = \mathcal{R}(\theta) \begin{pmatrix} 1 & 0 & 0 \\ \frac{3(\kappa + \sigma_1)}{3} & 0 & 0 \\ 0 & \frac{1}{3(\kappa + \sigma_2)} & 0 \\ 0 & 0 & \frac{1}{3(\kappa + \sigma_3)} \end{pmatrix} \mathcal{R}^{-1}(\theta), \tag{5}$$

where $K_{ii}(T)$ ($i = 1, 2, 3$) are nonlinear coefficients depending on the temperature solution, and $\mathcal{R}(\theta)$ is the rotation matrix given by

$$\mathcal{R}(\theta) = \begin{pmatrix} 1 & 0 & 0 \\ 0 & \cos \theta & -\sin \theta \\ 0 & \sin \theta & \cos \theta \end{pmatrix}.$$

Note that the nonlinearity in the SP₃ Eqs. (4) is supported by the fact that at high temperatures, the medium conductivity depends on the temperature and it should not be taken as a constant. In addition, by setting $\theta = 0$ in the rotation matrix, the Eqs. (4) yield the conventional SP₃ model proposed in [26]. In general, when the nonlinearity appears in the heat equation and not in the radiative transfer equation for which the asymptotic analysis is carried out, the SP₃ approximation originally proposed for linear isotropic problems is still valid for the nonlinear case. For the anisotropic problems, the asymptotic analysis can be carried out for each direction in the scattering tensor (*i.e.* for σ_1, σ_2 and σ_3 separately). In the current study, numerical simulations are carried out to show the performance of the mixed formulation for both linear and nonlinear cases.

3. Mixed finite element method

In the current study, Eqs. (4) are integrated in time using a second-order implicit backward differentiation formula (BDF2) also known as Gear scheme, see for example [2,6,7]. Thus, the time interval $[0, T_{final}]$ is divided into sub-intervals $[t_n, t_{n+1}]$ with length $\Delta t = t_{n+1} - t_n$ and we use the notation $u^n = u(\mathbf{x}, t_n)$ as the value of a generic function u at time t_n . We also discretize the three-dimensional domain Ω into a finite set of conforming elements \mathcal{T}_j ($j = 1, 2, \dots, N_e$) with N_e being the total number of elements. Here, the computational domain $\Omega_h \subseteq \Omega$ is the combination of all these finite elements. Hence, using (ϕ_1, ϕ_2, ϕ_3) as test functions, the weak formulation of the SP₃ Eqs. (4) reads as: Find $(T^{n+1}, \psi_1^{n+1}, \psi_2^{n+1}) \in V_h \times W_h \times W_h$, such that

$$\begin{cases} \int_{\Omega} \frac{3T^{n+1} - 4T^n + T^{n-1}}{2\Delta t} \phi_1 \, d\mathbf{x} + \int_{\Omega} \mathbf{K} \nabla T^{n+1} \cdot \nabla \phi_1 \, d\mathbf{x} \\ = \int_{\Omega} \frac{\kappa}{\tau^2} \left(\frac{\gamma_2 \psi_1^{n+1} - \gamma_1 \psi_2^{n+1}}{\gamma_2 - \gamma_1} - 4\pi B(T^{n+1}) \right) \phi_1 \, d\mathbf{x} + \\ \int_{\partial\Omega} \left(\frac{h_c}{\tau} (T_b - T^{n+1}) + \frac{\alpha\pi}{\tau} (B(T_b) - B(T^{n+1})) \right) \phi_1 \, d\mathbf{x}, \\ \tau^2 \mu_1^2 \int_{\Omega} \mathcal{E} \nabla \psi_1^{n+1} \cdot \nabla \phi_2 \, d\mathbf{x} + \int_{\Omega} \kappa \psi_1^{n+1} \phi_2 \, d\mathbf{x} = \int_{\Omega} 4\pi \kappa B(T^{n+1}) \phi_2 \, d\mathbf{x} \\ + \int_{\partial\Omega} \frac{\tau \mu_1^2}{3} (\eta_1 B(T_b) - \beta_2 \psi_2^{n+1} - \alpha_1 \psi_1^{n+1}) \phi_2 \, d\mathbf{x}, \\ \tau^2 \mu_2^2 \int_{\Omega} \mathcal{E} \nabla \psi_2^{n+1} \cdot \nabla \phi_3 \, d\mathbf{x} + \int_{\Omega} \kappa \psi_2^{n+1} \phi_3 \, d\mathbf{x} = \int_{\Omega} 4\pi \kappa B(T^{n+1}) \phi_3 \, d\mathbf{x} \\ + \int_{\partial\Omega} \frac{\tau \mu_2^2}{3} (\eta_2 B(T_b) - \beta_1 \psi_1^{n+1} - \alpha_2 \psi_2^{n+1}) \phi_3 \, d\mathbf{x}, \end{cases} \tag{6}$$

where V_h and W_h are the conforming finite element spaces. In this study, unlike the unified finite element methods for which both spaces V_h and W_h are the same, we propose different finite element discretizations for the temperature T and radiative solutions (ψ_1, ψ_2) . In fact, inspired by the mixed finite element method widely used for solving the Darcy and Navier–Stokes equations, we propose a mixed finite element formulation where the finite element spaces V_h and W_h are defined by

$$\begin{aligned} V_h &= \{T_h \in C^0(\overline{\Omega}) : T_h|_{\mathcal{T}} \in \mathbb{P}_m(\mathcal{T}), \quad \forall \mathcal{T} \in \Omega_h\}, \\ W_h &= \{\psi_h \in C^0(\overline{\Omega}) : \psi_h|_{\mathcal{T}} \in \mathbb{P}_{m-1}(\mathcal{T}), \quad \forall \mathcal{T} \in \Omega_h\}, \end{aligned}$$

where $\mathbb{P}_m(\mathcal{T})$ and $\mathbb{P}_{m-1}(\mathcal{T})$ are polynomial spaces defined in the finite element \mathcal{T} of degree m and $m-1$, respectively. Notice that, we also compare the proposed mixed formulation to its unified counterparts widely used in the literature where the finite element spaces V_h and W_h are the same defined as

$$V_h = W_h = \{T_h \in C^0(\overline{\Omega}) : T_h|_{\mathcal{T}} \in \mathbb{P}_m(\mathcal{T}), \quad \forall \mathcal{T} \in \Omega_h\}.$$

It is well known that most mixed finite element formulations face numerical stability issues if function spaces for their unknowns are not chosen consistently. Typically, spurious oscillations in the numerical solution may arise and affect the accuracy of the method. The theory of mixed finite element formulations [10] provides compatibility conditions on spaces to ensure the numerical stability of the problem. Here, the SP_3 approximation fits into the classical framework of perturbed saddle-point problems. Therefore, it ensures the stability conditions relevant to this class of problems, following closely Brezzi's classical treatment [10]. It is also possible to describe the inf-sup test [12], which is a numerical test widely used for checking the compatibility of specific functions spaces in the discrete formulation. It should also be noted that the mixed finite element method proposed in this study should not be confused with the one used for solving the incompressible Navier–Stokes equations, the Darcy equations or linear elasticity problems. In those problems, the governing equations are coupled through a differential operator such as the gradient of the pressure in the Navier–Stokes equations and conditions as those reported in [5,11] are required to ensure stability in the mixed finite element methods. In our case, the coupling between the heat conduction equation and the SP_3 equations is through polynomial functions at the right-hand side of each equation in (4). Therefore, there will be no stability issues related to the low-order elements of the radiative solutions because only a source function needs to be evaluated at those elements and no differential operator in the heat equation is affected by these low-order elements. This has clearly been confirmed in the numerical results presented in this study for both linear and nonlinear SP_3 equations. Note that the finite element discretization of the weak form (6) is trivial and for brevity in the presentation it is omitted here. In our simulations presented in the current study for the SP_3 model, we consider linear \mathbb{P}_1 , quadratic \mathbb{P}_2 and cubic \mathbb{P}_3 finite elements as depicted in Fig. 1 for both unified and mixed discretizations. To solve the nonlinear systems (6), the Newton's method is used at each timestep. The linear systems resulting from the Newton's method are solved by an incomplete LU decomposition GMRES solver from the PETSc¹ library, see for example [4,35]. The convergence of the Newton's iterations was achieved when the residual norm is less than 10^{-6} . For all numerical results presented in this study, three to five iterations were sufficient to achieve this required convergence.

4. Numerical results and examples

In this section we examine the accuracy and the reliability of the mixed finite element method proposed in this study using examples of radiation–conduction problems in three-dimensional enclosures. In the first example, quantitative results are examined for a radiation–conduction problem with known analytical solutions. Comparisons between results obtained using both unified and mixed finite elements for the SP_3 model are presented for a radiation–conduction problem in isotropic media. The third example examines the performance of the proposed method for solving a nonlinear radiation–conduction problem in anisotropic media. All the computations are performed on a Dell Precision 7920 Tower with 20C Dual Intel Xeon Gold 6148 2.4 GHz processor and 64 GB 2666 MHz DDR4 Memory.

4.1. Accuracy example

In this example, we investigate the performance of unified and mixed discretizations with the considered finite elements for a problem with known exact solutions. Here, a manufactured solution of the model (4) is reconstructed by adding extra source functions in the right-hand side of the equations which are determined such that the analytical solutions are given by

$$\begin{aligned} T(x, y, z, t) &= \sin(2\pi x) \sin(2\pi y) \sin(2\pi z) \exp(t), \\ \psi_1(x, y, z, t) &= \tanh(T + 1), \\ \psi_2(x, y, z, t) &= \tanh(T - 1). \end{aligned} \tag{7}$$

This problem is solved in the unit cube $\Omega = [0, 1] \times [0, 1] \times [0, 1]$ and the initial temperature and boundary functions are also calculated according to the exact solutions in (7). Here, the absorption coefficient $\kappa = 1$, the scattering coefficient $\sigma_1 = \sigma_2 = \sigma_3 = 0$, the anisotropy angle $\theta = 0$, the surface emissivity $\alpha = 0$, the optical scale $\tau = 1$, and the heat conductivity $\mathbf{K} = \mathbf{I}$, with \mathbf{I} is the unity matrix. A fixed timestep $\Delta t = 0.001$ is used in the simulations and the obtained results are displayed at the final time $T_{final} = 0.1$.

¹ <http://www.mcs.anl.gov/petsc/>.

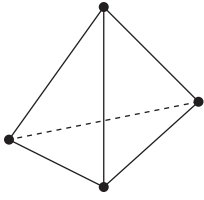
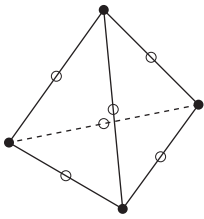
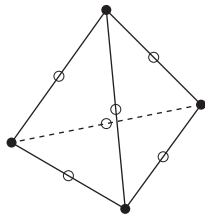
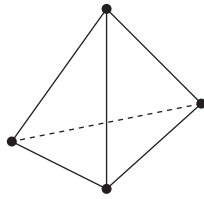
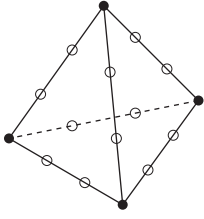
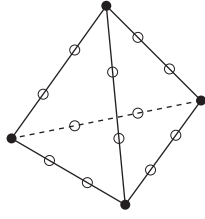
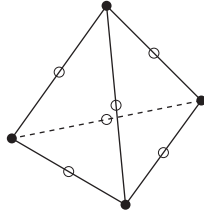
Unified discretization	Mixed discretization	
 <p data-bbox="336 493 531 522">\mathbb{P}_1 for T, ψ_1 and ψ_2</p>		
 <p data-bbox="336 825 531 854">\mathbb{P}_2 for T, ψ_1 and ψ_2</p>	 <p data-bbox="758 825 837 854">\mathbb{P}_2 for T</p>	 <p data-bbox="1006 825 1172 854">\mathbb{P}_1 for ψ_1 and ψ_2</p>
 <p data-bbox="336 1162 531 1192">\mathbb{P}_3 for T, ψ_1 and ψ_2</p>	 <p data-bbox="758 1162 837 1192">\mathbb{P}_3 for T</p>	 <p data-bbox="1006 1162 1172 1192">\mathbb{P}_2 for ψ_1 and ψ_2</p>

Fig. 1. Unified and mixed finite elements used for the discretization of SP_3 equations.

Our aim in this test example is to present the convergence rates of the proposed mixed finite element method and compare these convergence results to those obtained using its unified counterparts. To this end we define the relative error as

$$L^2\text{-error} = \frac{\|T_{ex} - T_{num}\|_{L^2(\Omega)}}{\|T_{ex}\|_{L^2(\Omega)}},$$

where T_{ex} and T_{num} are the exact and numerical solutions, respectively. The obtained convergence plots are presented in Fig. 2 for the considered finite elements. Obviously, refining the spatial discretization improves the accuracy in both unified and mixed finite element methods. In addition, high-order accuracy is ensured when using the high-order \mathbb{P}_3 finite elements in the simulation. As can be seen from these plots, the expected convergence order is achieved for each corresponding discretization in the considered finite element method. Note that these numerical results need to be supported by a rigorous analysis of convergence and error estimates for the proposed mixed finite element method. However, the purpose of the present study is on the computational assessment of the mixed finite element method for solving three-dimensional SP_3 approximations of radiation–conduction in optically thick anisotropic media and its analysis will be addressed in a future work.

Next we examine the efficiency of the proposed mixed method for this problem. Table 2 summarizes the obtained errors and computational costs for each timestep using the proposed discretizations. It is evident that the error using

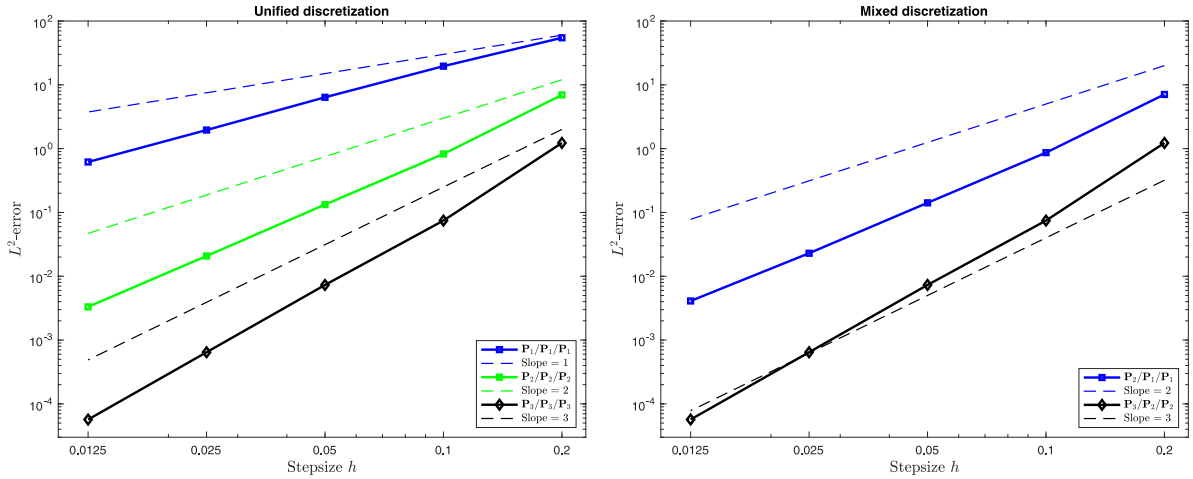


Fig. 2. Convergence plots obtained using the unified discretization (left) and mixed discretization (right) for the accuracy example.

Table 2

Errors and computational costs obtained using the unified and mixed discretizations with the considered finite elements for the accuracy example. Here, CPU times are given in seconds.

Unified discretization		
Finite elements	L^2 -error	CPU time
$\mathbb{P}_1/\mathbb{P}_1/\mathbb{P}_1$	7.6426E-03	77
$\mathbb{P}_2/\mathbb{P}_2/\mathbb{P}_2$	8.1175E-05	219
$\mathbb{P}_3/\mathbb{P}_3/\mathbb{P}_3$	2.5152E-06	1428
Mixed discretization		
$\mathbb{P}_2/\mathbb{P}_1/\mathbb{P}_1$	8.9647E-05	116
$\mathbb{P}_3/\mathbb{P}_2/\mathbb{P}_2$	2.5164E-06	482

\mathbb{P}_2 for T and \mathbb{P}_2 for ψ_1 and ψ_2 , referred to in the table as $\mathbb{P}_2/\mathbb{P}_2/\mathbb{P}_2$ discretization, is almost the same as the error using \mathbb{P}_2 for T and \mathbb{P}_1 for ψ_1 and ψ_2 , referred to in the table as $\mathbb{P}_2/\mathbb{P}_1/\mathbb{P}_1$ discretization. Similarly, the error using \mathbb{P}_3 for T and \mathbb{P}_3 for ψ_1 and ψ_2 , referred to in the table as $\mathbb{P}_3/\mathbb{P}_3/\mathbb{P}_3$ discretization is almost the same as the error using \mathbb{P}_3 for T and \mathbb{P}_2 for ψ_1 and ψ_2 , referred to in the table as $\mathbb{P}_3/\mathbb{P}_2/\mathbb{P}_2$. However, the computational time using the mixed finite elements $\mathbb{P}_2/\mathbb{P}_1/\mathbb{P}_1$ or $\mathbb{P}_3/\mathbb{P}_2/\mathbb{P}_2$ finite elements is much smaller compared to the computational time using the unified $\mathbb{P}_2/\mathbb{P}_2/\mathbb{P}_2$ or $\mathbb{P}_3/\mathbb{P}_3/\mathbb{P}_3$ finite elements, respectively. For instance, using the mixed finite elements $\mathbb{P}_3/\mathbb{P}_2/\mathbb{P}_2$ produces the same accuracy as using the unified finite elements $\mathbb{P}_3/\mathbb{P}_3/\mathbb{P}_3$ in terms of errors but with a computational time about 3 times lower. This clearly shows that the proposed mixed finite element method is more suitable for a fast and accurate solution of the SP_3 model compared to the unified finite element method.

4.2. Radiation–conduction problem in isotropic media

To examine the performance of the proposed mixed formulation on a radiative heat transfer example, we consider the benchmark problem widely used in the literature for modeling cooling materials such as glass, see [24,37] among others. Thus, we solve the coupled radiation–conduction problem (4) in the computational domain $\Omega = [0, 1] \times [0, 1] \times [0, 1]$ subject to an initial temperature $T_0 = 1500$ K and a boundary temperature $T_b = 300$ K. The remaining parameters are selected as $h_c = 1$, $\kappa = 1$, $\sigma_1 = \sigma_2 = \sigma_3 = 0$, $\theta = 0$, and $\tau = 1$. The medium is assumed to be isotropic for which the heat conductivity $\mathbf{K} = \mathbf{I}$, with \mathbf{I} is the unity matrix and the surface emissivity is set to zero. In all results presented for this example, a time step fixed to $\Delta t = 10^{-6}$ and a structured mesh with step size $h = 0.025$ are used in the simulations. Computational results are presented at three different instants using both unified and mixed finite elements.

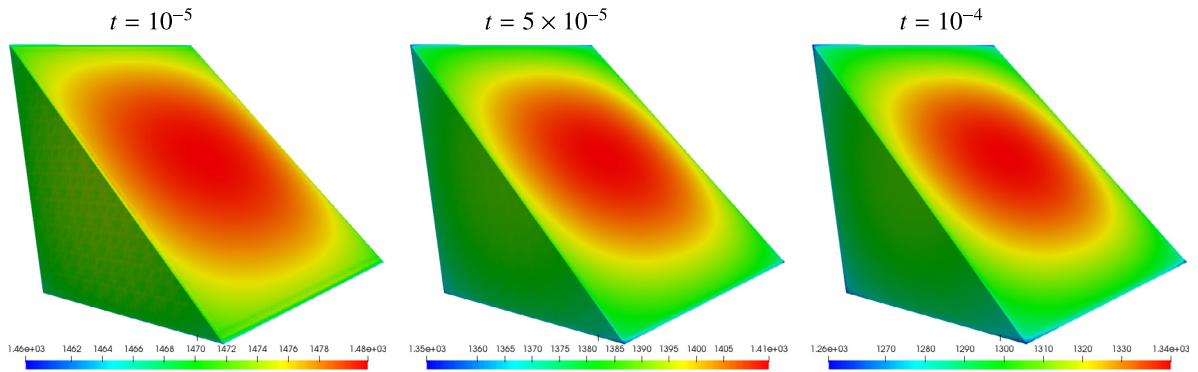


Fig. 3. Snapshots of the temperature obtained using the mixed $\mathbb{P}_2/\mathbb{P}_1/\mathbb{P}_1$ discretization at three different instants for the radiation–conduction problem in isotropic media.

Table 3

Mesh statistics, errors and computational costs obtained using the unified and mixed discretizations with the considered finite elements for the radiation–conduction problem in isotropic media. Here, CPU times are given in minutes.

Unified discretization			
Finite elements	# DoFs	Error	CPU time
$\mathbb{P}_1/\mathbb{P}_1/\mathbb{P}_1$	206 763	27.5259	1.2
$\mathbb{P}_2/\mathbb{P}_2/\mathbb{P}_2$	1 594 323	8.5857	21
$\mathbb{P}_3/\mathbb{P}_3/\mathbb{P}_3$	2 981 883	5.8735	140
Mixed discretization			
$\mathbb{P}_2/\mathbb{P}_1/\mathbb{P}_1$	669 283	8.5127	2.5
$\mathbb{P}_3/\mathbb{P}_2/\mathbb{P}_2$	2 056 843	5.8612	43

As in this previous example, different discretizations are investigated to assess the difference between the mixed and unified formulations. Here, we consider $\mathbb{P}_3/\mathbb{P}_3/\mathbb{P}_3$, $\mathbb{P}_3/\mathbb{P}_2/\mathbb{P}_2$, $\mathbb{P}_2/\mathbb{P}_2/\mathbb{P}_2$, $\mathbb{P}_2/\mathbb{P}_1/\mathbb{P}_1$, and $\mathbb{P}_1/\mathbb{P}_1/\mathbb{P}_1$ finite elements. The number of degrees of freedom (#DoFs) associated with these discretizations is listed in Table 3. It is evident that the number of degrees of freedom in the mixed $\mathbb{P}_2/\mathbb{P}_1/\mathbb{P}_1$ and $\mathbb{P}_3/\mathbb{P}_2/\mathbb{P}_2$ discretizations is lower than their unified counterparts $\mathbb{P}_2/\mathbb{P}_2/\mathbb{P}_2$ and $\mathbb{P}_3/\mathbb{P}_3/\mathbb{P}_3$, respectively. Obviously, this reduction in the number of degrees of freedom has an impact on the computational cost required for each discretization. In Fig. 3 we present distributions of the temperature obtained using the mixed $\mathbb{P}_2/\mathbb{P}_1/\mathbb{P}_1$ finite elements at three different times namely $t = 10^{-5}$, 5×10^{-5} and 10^{-4} . Notice that for a better insight, only part of the computational domain is illustrated in Fig. 3. It should also be noted that similar temperature distributions are obtained using the mixed $\mathbb{P}_3/\mathbb{P}_2/\mathbb{P}_2$ finite elements and therefore are not included here. It is clear from the computed results in Fig. 3 that the heat patterns formed in the domain along with the cooling process are well captured. There is also a good agreement with these results to those reported in [24,37] for a similar radiative heat transfer problem. It is worth remarking that all these thermal features are achieved by solving systems of algebraic equations smaller than those required for the unified discretizations using $\mathbb{P}_2/\mathbb{P}_2/\mathbb{P}_2$ and $\mathbb{P}_3/\mathbb{P}_3/\mathbb{P}_3$ finite elements.

To further quantify the computational results for this example, we calculate the difference between the solutions obtained using the considered discretizations as

$$\text{Error} = \|T_{ref} - T_{num}\|_{L^2(\Omega)},$$

where T_{ref} is the reference solution obtained on a fine mesh with 57 83 853 degrees of freedom using the $\mathbb{P}_3/\mathbb{P}_3/\mathbb{P}_3$ discretization, and T_h is the numerical solution obtained using the other different discretizations. Table 3 summarizes the obtained results for errors and computational costs by the considered unified and mixed discretizations at time $t = 5 \times 10^{-5}$. Clearly, the errors obtained using the unified $\mathbb{P}_3/\mathbb{P}_3/\mathbb{P}_3$ and $\mathbb{P}_2/\mathbb{P}_2/\mathbb{P}_2$ discretizations are almost the same as those errors obtained using the mixed $\mathbb{P}_3/\mathbb{P}_2/\mathbb{P}_2$ and $\mathbb{P}_2/\mathbb{P}_1/\mathbb{P}_1$ discretizations, respectively. However, the

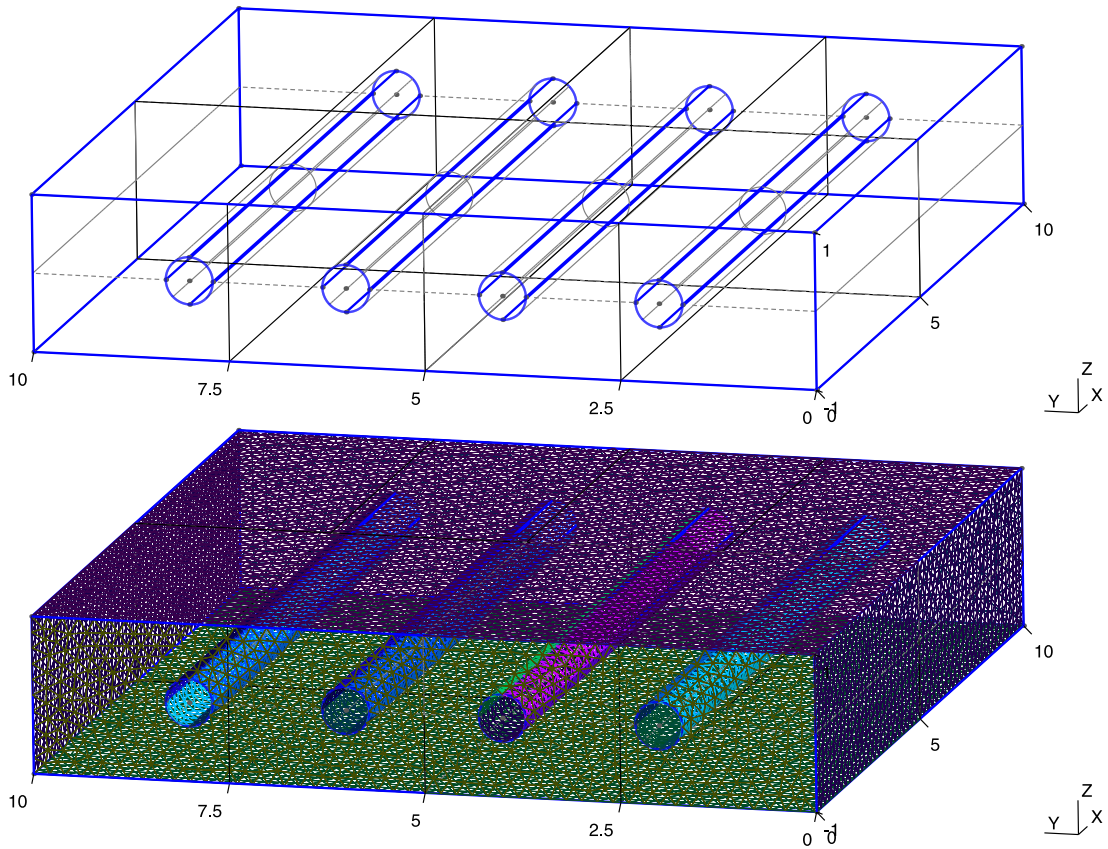


Fig. 4. Domain configuration (top plot) and computational mesh (bottom plot) for the radiation–conduction problem in anisotropic media.

CPU time using the mixed $\mathbb{P}_2/\mathbb{P}_1/\mathbb{P}_1$ or $\mathbb{P}_3/\mathbb{P}_2/\mathbb{P}_2$ discretizations is far smaller compared to the CPU time using the unified $\mathbb{P}_2/\mathbb{P}_2/\mathbb{P}_2$ or $\mathbb{P}_3/\mathbb{P}_3/\mathbb{P}_3$ discretizations, respectively. This saving in the computational cost shows that for a similar accuracy, the mixed finite elements are more suitable for the SP_3 model compared to the unified finite elements. In addition, differences in the results obtained for the unified $\mathbb{P}_2/\mathbb{P}_2/\mathbb{P}_2$ and $\mathbb{P}_3/\mathbb{P}_3/\mathbb{P}_3$ finite elements are less than 8.5% and 5.8%, respectively. Using the mixed $\mathbb{P}_2/\mathbb{P}_1/\mathbb{P}_1$ and $\mathbb{P}_3/\mathbb{P}_2/\mathbb{P}_2$ finite elements, these differences remain roughly the same. Furthermore, the computational time required for the proposed mixed $\mathbb{P}_3/\mathbb{P}_2/\mathbb{P}_2$ finite elements, is 69% less than the time required for $\mathbb{P}_3/\mathbb{P}_3/\mathbb{P}_3$ finite elements, while the implementation using the mixed $\mathbb{P}_2/\mathbb{P}_1/\mathbb{P}_1$ finite elements reduces this computational cost to 98%. As a result, the mixed $\mathbb{P}_2/\mathbb{P}_1/\mathbb{P}_1$ finite element method is considered as a good candidate for obtaining accurate and efficient numerical results for solving coupled radiation–convection problems.

4.3. Nonlinear radiation–conduction problem in anisotropic media

Our final example consists of a nonlinear radiation–conduction problem in an anisotropic plate including four hollow cylinders modeling for example embedded pipes for radiant cooling and heating systems. Here, we solve the Eqs. (4) in a plate domain $\Omega = [0, 10] \times [0, 10] \times [-1, 1]$ as illustrated in Fig. 4. The four cylinders span the whole lateral distance with the same radius of 0.3 equidistantly distributed in the plate with their centers located at $(0, 2, 0)$, $(0, 4, 0)$, $(0, 6, 0)$ and $(0, 8, 0)$. In our simulations, the scattering coefficients $\sigma_1 = 0$, $\sigma_2 = 0.1$, and $\sigma_3 = 0$, the absorption coefficient $\kappa = 1$, the convective heat transfer $h_c = 1$, the surface emissivity $\alpha = 0.01$, the diffusion scale $\tau = 1$, and the thermal conductivity \mathbf{K} is assumed to be nonlinear and anisotropic defined by (5) with

$$K_{11}(T) = 0.1 + 0.02T + 0.0005T^2, \quad K_{22}(T) = 0.1 + 0.02T, \quad K_{33}(T) = 0.1 + 0.02T + 0.0005T^2,$$

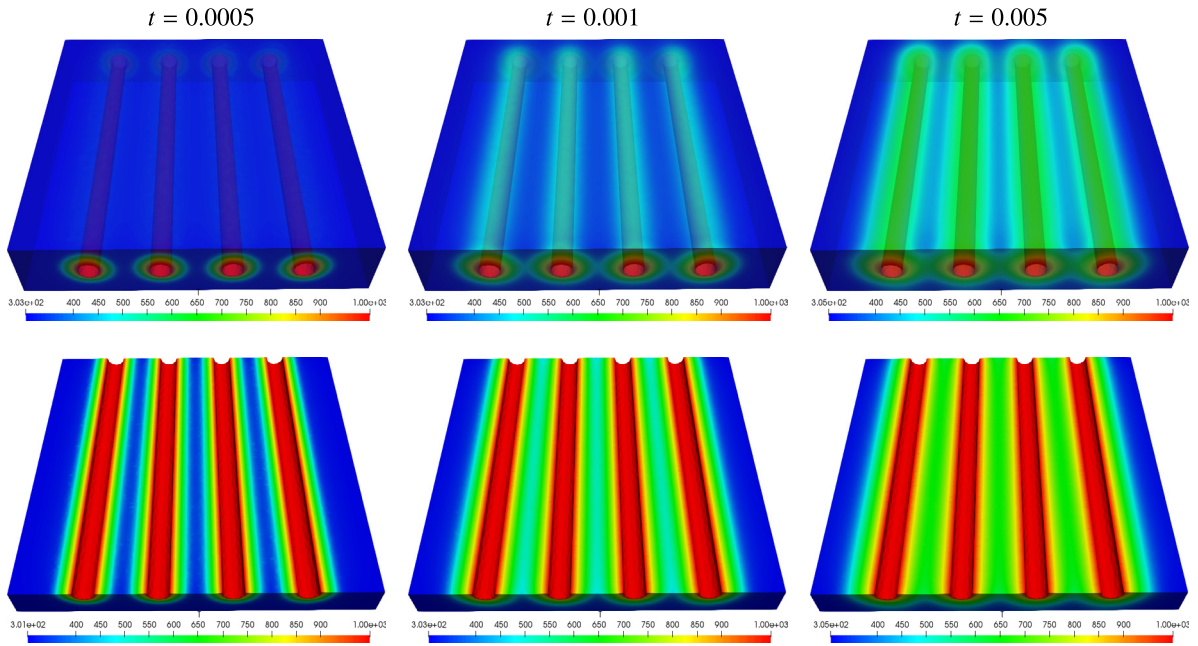


Fig. 5. Temperature distribution in the entire plate (top plots) and in the plane $z = 0$ (bottom plots) obtained at three different instants for the radiation–conduction problem in anisotropic media.

and the anisotropy angle $\theta = \frac{\pi}{4}$. On the boundaries of the domain we use Dirichlet-type conditions with fixed temperature $T_b = 1000$ K on the surface of the cylinders whereas Robin-type conditions with $T_b = 300$ K are employed on the other surfaces of the plate. The initial temperature is set to $T_0 = 1000$ K, the time step $\Delta t = 10^{-5}$ and the computed results are displayed at three different times using an unstructured mesh with 1 08 884 tetrahedrals as shown in Fig. 4. It should be pointed out that the main objective of this example is to examine the performance of the proposed mixed finite element method for solving nonlinear three-dimensional radiation–conduction problems in anisotropic media. To this end we consider the mixed $\mathbb{P}_2/\mathbb{P}_1/\mathbb{P}_1$ finite elements and the obtained results are compared to those obtained using the unified $\mathbb{P}_1/\mathbb{P}_1/\mathbb{P}_1$ and $\mathbb{P}_2/\mathbb{P}_2/\mathbb{P}_2$ finite elements. Hence, the total numbers of degrees of freedom are 496 596, 211 274 and 68 613 for the discretizations using $\mathbb{P}_2/\mathbb{P}_2/\mathbb{P}_2$, $\mathbb{P}_2/\mathbb{P}_1/\mathbb{P}_1$ and $\mathbb{P}_1/\mathbb{P}_1/\mathbb{P}_1$ finite elements, respectively.

Fig. 5 depicts snapshots of the temperature in the plate obtained using the $\mathbb{P}_2/\mathbb{P}_1/\mathbb{P}_1$ finite elements at three different instants $t = 0.0005, 0.001$ and 0.005 along with parts of the plate at $z = 0$ for a better visualization. As expected, the heat released from the hot cylinder walls is transferred inside the plate and covers the whole plate as the time progresses. At earlier times, steep thermal gradients are also detected in the domain due to the difference between the heat isolation boundary conditions and the high heat release rates near the cylinder walls. Despite using a relatively coarse mesh, the proposed mixed $\mathbb{P}_2/\mathbb{P}_1/\mathbb{P}_1$ finite elements accurately captures these steep gradients and their changes in time. Notice that results obtained using the unified $\mathbb{P}_2/\mathbb{P}_2/\mathbb{P}_2$ finite elements reveal the same thermal structures and therefore are not included in Fig. 5.

Comparison between the considered mixed and unified discretizations is also carried out for this nonlinear radiation–conduction problem in anisotropic media. In Fig. 6 we present one-dimensional cross-sections of the temperature at $x = z = 0$ obtained using the unified $\mathbb{P}_1/\mathbb{P}_1/\mathbb{P}_1$ and $\mathbb{P}_2/\mathbb{P}_2/\mathbb{P}_2$ finite elements compared to the mixed $\mathbb{P}_2/\mathbb{P}_1/\mathbb{P}_1$ finite elements at time $t = 0.001$. For comparison reasons, differences between these results are also included in the plots shown in Fig. 6. Noticeably, results obtained using the $\mathbb{P}_1/\mathbb{P}_1/\mathbb{P}_1$ finite elements are less accurate than those obtained using the $\mathbb{P}_2/\mathbb{P}_2/\mathbb{P}_2$ finite elements with a maximum difference of 50 K. On the other hand, the temperature profiles obtained using the $\mathbb{P}_2/\mathbb{P}_2/\mathbb{P}_2$ and $\mathbb{P}_2/\mathbb{P}_1/\mathbb{P}_1$ finite elements are very similar with a maximum difference less than 4 K. This confirms that the mixed $\mathbb{P}_2/\mathbb{P}_1/\mathbb{P}_1$ formulation is the most suitable discretization for the SP_3 model since the results obtained using the mixed $\mathbb{P}_2/\mathbb{P}_1/\mathbb{P}_1$ finite elements are as accurate

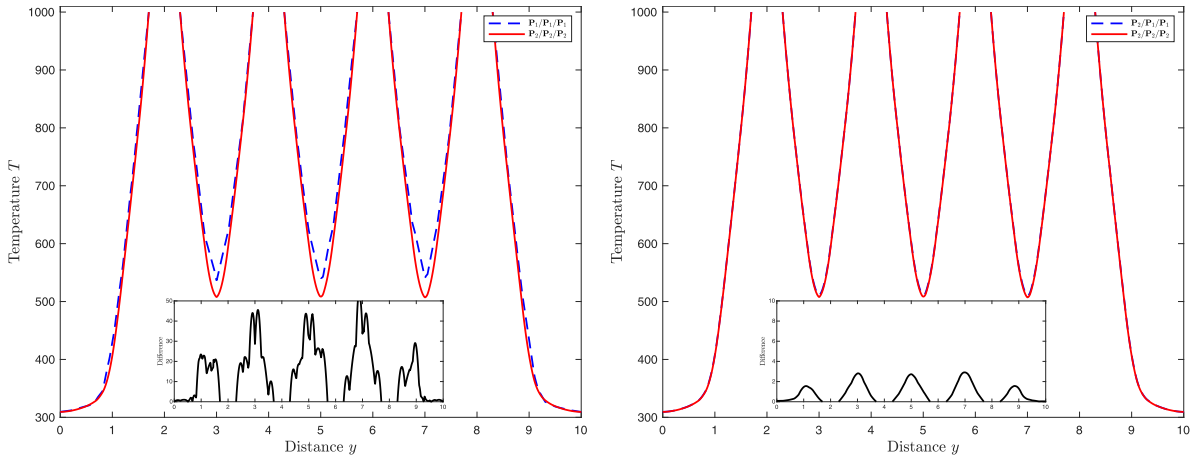


Fig. 6. Comparison between the unified discretizations (left plot) and the mixed discretizations (right plot) obtained at time $t = 0.001$ for the radiation–conduction problem in anisotropic media.

as those obtained using the unified $\mathbb{P}_2/\mathbb{P}_2/\mathbb{P}_2$ finite elements but with a computational cost more than two times faster. Note that the results obtained for this heat transfer problem also confirm the previous conclusions about the efficiency and accuracy of the mixed finite elements. Indeed, the proposed mixed $\mathbb{P}_2/\mathbb{P}_1/\mathbb{P}_1$ finite element method as can be seen in the results shown in Figs. 5 and 6 performs very well. The temperature solution in this case is highly accurate and stable even on a relatively coarse mesh. It should also be mentioned that the efficiency of the proposed mixed finite element method is reflected in the reduction in the total number of degrees of freedom and the reduction in the size of associated systems of algebraic equations required to be solved at each time step to update the solution. Finally, we also note that the proposed mixed finite element method is highly attractive for computational heat transfer.

Our next concern with this example is to examine the performance of the proposed mixed $\mathbb{P}_2/\mathbb{P}_1/\mathbb{P}_1$ finite elements for different anisotropic conditions for this radiation–conduction problem. For this end we run the simulations for three different anisotropy angles $\theta = 0, \frac{\pi}{6}$ and $\frac{\pi}{2}$, and the obtained temperature distributions at time $t = 0.001$ are displayed in Fig. 7. For the considered anisotropy conditions, the heat exhibits different patterns for each value of the angle θ . Higher heat release is observed in the plate for larger values of the anisotropy angle and the proposed mixed finite element method accurately resolves these thermal features with no spurious oscillations or excessive numerical diffusion. This can also be seen in the temperature profiles at $x = z = 0$ presented in Fig. 8 for $\theta = 0, \frac{\pi}{6}, \frac{\pi}{4}, \frac{\pi}{3}$ and $\frac{\pi}{2}$. Furthermore, steeper thermal gradients appear at the vicinity of cylinder walls for small values of the anisotropy angle and as the angle increases higher temperatures are released with smoother boundary layers at these walls. It should also be noted that this resolution is captured on a relatively coarse mesh and without any mesh refinements implemented at the cylinder walls.

5. Conclusions

A new mixed finite element method has been developed for solving nonlinear radiation–conduction equations in optically thick anisotropic media. Under the assumption that the medium is optically thick, the integro-differential equation for radiative transfer is asymptotically approximated by the SP_3 model. This results in a coupled system of one parabolic-type equation for the temperature distribution and two elliptic-type equations for the radiative field. We assumed nonlinear anisotropic conductivity depending on the temperature and both the direction and location coordinates. The proposed mixed finite element method consists of using different spaces for the discretization of temperature and radiative solutions. Here, we used mixed $\mathbb{P}_m/\mathbb{P}_{m-1}/\mathbb{P}_{m-1}$ finite elements for which high-order elements \mathbb{P}_m are used for the temperature solution and the low-order elements \mathbb{P}_{m-1} are used for the radiative solutions. This is supported by the fact that the solution of interest in most applications of radiative heat transfer in optically thick media is the temperature. The performance of the proposed mixed finite element

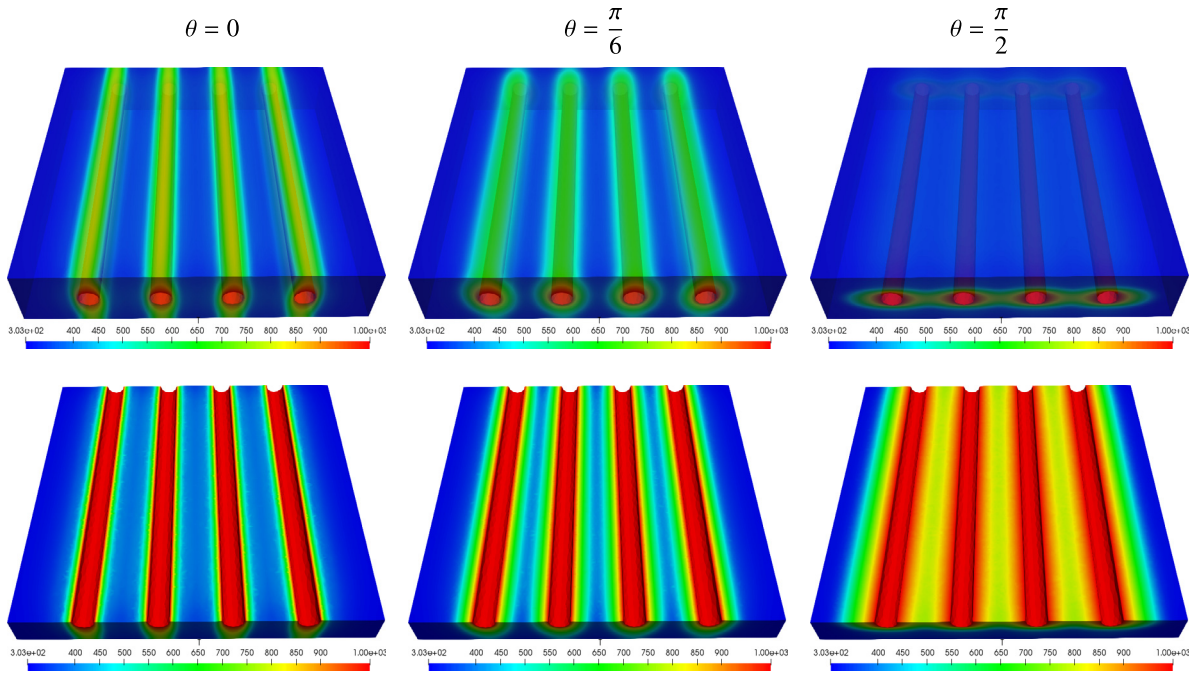


Fig. 7. Temperature distribution in the entire plate (top plots) and in the plane $z = 0$ (bottom plots) obtained at time $t = 0.001$ using three different anisotropy angles for the radiation–conduction problem in anisotropic media.

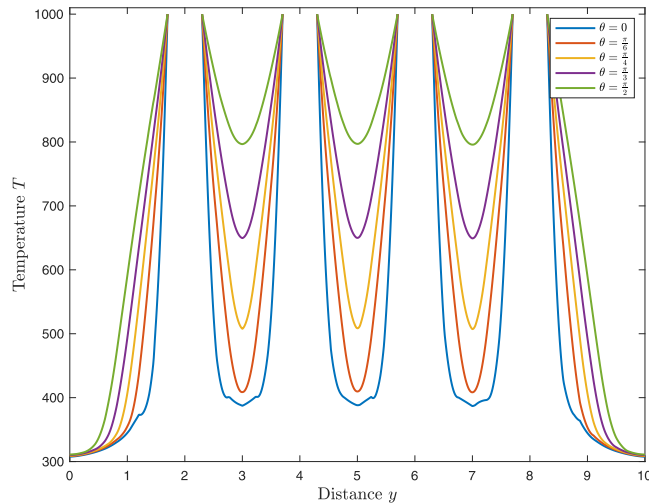


Fig. 8. Temperature profiles obtained at time $t = 0.001$ using different anisotropy angles for the radiation–conduction problem in anisotropic media.

method has been examined using various test examples of radiation–conduction problems in three-dimensional enclosures. The obtained numerical results using the mixed finite element method confirm a significant reduction in the computational cost compared to the results using the unified finite element method at the same accuracy. Furthermore, results obtained for the considered examples have also shown the capabilities of the proposed mixed finite element method in simulations of complex radiative heat transfer applications in three space dimensions using unstructured tetrahedral meshes. Future work will concentrate on the extension of the mixed finite element

method to coupled problems of flow and radiative heat transfer in non-gray participating anisotropic media. It should be stressed that the emphasis of the present has been exclusively on the computational assessment of the proposed mixed finite element method for solving three-dimensional radiation–conduction equations in optically thick anisotropic media. However, using the compatibility conditions on the finite element spaces proposed in [10] and following the arguments reported in [12], it is possible to establish a theoretical analysis of convergence and stability for the proposed mixed formulation. Results on this analysis along with error estimates will be carried out separately in a future work.

Acknowledgments

The authors wish to acknowledge the financial support provided by the Royal Society, United Kingdom under the contract IES-R2-202078 and the financial support provided by the American University of Sharjah, United Arab Emirates. The work in this paper was supported, in part, by the Open Access Program from the American University of Sharjah. This paper represents the opinions of the author(s) and does not mean to represent the position or opinions of the American University of Sharjah.

References

- [1] J. Albadr, M. El-Amrani, M. Seaid, Simplified finite element approximations for coupled natural convection and radiation heat transfer, *Numer. Heat Transfer A* (2022) 1–25.
- [2] M. Alqasemi, Y. Belhamadia, A semi-implicit backward differentiation ADI method for solving monodomain model, in: *Computational Science – ICCS 2021*, Springer International Publishing, Cham, 2021, pp. 541–548.
- [3] R. Backofen, T. Bilz, A. Ribalta, A. Voigt, SP_N -Approximations of internal radiation in crystal growth of optical materials, *J. Cryst. Growth* 266 (2004) 264–270.
- [4] S. Balay, K. Buschelman, V. Eijkhout, W. Gropp, D. Kaushik, M. Knepley, L.C. McInnes, B. Smith, H. Zhang, *PETSc Users Manual*, Tech. Rep. ANL-95/11-Revision 2.1.6, Argonne National Laboratory, Argonne, Illinois, 2003.
- [5] K.J. Bathe, F. Brezzi, Stability of finite element mixed interpolations for contact problems, *Atti Accad. Naz. Linc. Cl. Sci. Fis. Mat. Nat. Rend. Lincei. Mat. Appl.* 12 (3) (2001) 167–183.
- [6] Y. Belhamadia, A time-dependent adaptive remeshing for electrical waves of the heart, *IEEE Trans. Biomed. Eng.* 55 (2) (2008) 443–452.
- [7] Y. Belhamadia, T. Briffard, A. Fortin, Efficiency of parallel anisotropic mesh adaptation for the solution of the bidomain model in cardiac tissue, *J. Comput. Sci.* 61 (2022) 101656.
- [8] Y. Belhamadia, G.O. Cassol, S. Dubljevic, Numerical modelling of hyperbolic phase change problems: Application to continuous casting, *Int. J. Heat Mass Transfer* 209 (2023) 124042.
- [9] Y. Belhamadia, M. Seaid, Computing enhancement of the nonlinear SP_N approximations of radiative heat transfer in participating material, *J. Comput. Appl. Math.* 434 (2023) 115342, <http://dx.doi.org/10.1016/j.cam.2023.115342>.
- [10] D. Boffi, F. Brezzi, M. Fortin, et al., *Mixed Finite Element Methods and Applications*, Vol. 44, Springer, 2013.
- [11] F. Brezzi, M. Fortin, A minimal stabilisation procedure for mixed finite element methods, *Numer. Math.* 89 (2001) 457–491.
- [12] D. Chapelle, K.-J. Bathe, The inf-sup test, *Comput. Struct.* 47 (4–5) (1993) 537–545.
- [13] S. Dhurandhar, A. Bansal, S. Boppudi, K. Murty, D. Medha, Application and comparative analysis of radiative heat transfer models for coal-fired furnace, *Numer. Heat Transfer A* 82 (4) (2022) 137–168.
- [14] F. Fan, D. Xu, Y. Zhu, G. Tan, D. Zhao, A simple, accurate, and universal method for characterizing and comparing radiative cooling materials and devices, *Int. J. Heat Mass Transfer* 200 (2023) 123494.
- [15] M. Frank, M. Seaid, J. Janicka, A. Klar, R. Pinnau, G. Thömmes, A comparison of approximate models for radiation in gas turbines, *Int. J. Prog. CFD* 3 (2004) 191–197.
- [16] M. Galtier, W. Woelffel, F. André, V. Solovjov, B. Webb, S. Roy, Assessment of narrow-band and full spectrum gas radiation methods in a real industrial glass furnace configuration, *Appl. Therm. Eng.* 216 (2022) 119020.
- [17] W. Ge, C. David, M. Modest, R. Sankaran, S. Roy, Comparison of spherical harmonics method and discrete ordinates method for radiative transfer in a turbulent jet flame, *J. Quant. Spectrosc. Radiat. Transfer* 296 (2023) 108459.
- [18] E. Gelbard, *Simplified Spherical Harmonics Equations and Their Use in Shielding Problems*, Tech. Rep., Westinghouse Electric Corp. Bettis Atomic Power Lab., Pittsburgh, 1961.
- [19] S. Giani, M. Seaid, hp -Adaptive discontinuous Galerkin methods for simplified PN approximations of frequency-dependent radiative transfer, *Comput. Methods Appl. Mech. Engrg.* 301 (2016) 52–79.
- [20] S. Giani, M. Seaid, hp -adaptive discontinuous Galerkin methods for simplified P_N approximations of frequency-dependent radiative transfer, *Comput. Methods Appl. Mech. Engrg.* 301 (2016) 52–79.
- [21] S. Giani, M. Seaid, Multi- hp adaptive discontinuous Galerkin methods for simplified PN approximations of 3D radiative transfer in non-gray media, *Appl. Numer. Math.* 150 (2020) 252–273.
- [22] G. Goertzel, The method of discrete ordinates, *Nucl. Sci. Eng.* 4 (4) (1958) 581–587.
- [23] T. Götz, Coupling heat conduction and radiative transfer, *J. Quant. Spectrosc. Radiat. Transfer* 72 (1) (2002) 57–73.

- [24] A. Klar, J. Lang, M. Seaid, Adaptive solutions of SP_N -approximations to radiative heat transfer in glass, *Int. J. Therm. Sci.* 44 (11) (2005) 1013–1023.
- [25] E. Larsen, J. Morel, J. McGhee, Asymptotic derivation of the multigroup P1 and simplified PN equations with anisotropic scattering, *Nucl. Sci. Eng.* 123 (3) (1996) 328–342.
- [26] E. Larsen, G. Thömmes, A. Klar, M. Seaid, T. Götz, Simplified P_N approximations to the equations of radiative heat transfer and applications, *J. Comput. Phys.* 183 (2) (2002) 652–675.
- [27] D. Mazumdar, Review, analysis, and modeling of continuous casting tundish systems, *Steel Res. Int.* 90 (4) (2019) 1800279.
- [28] M. Mirzaee, A. Zolfaghari, A. Minuchehr, Reactor core analysis through the SP3-ACMFD approach. Part I: Static solution, *Nucl. Eng. Technol.* 52 (2) (2020) 223–229.
- [29] M. Modest, *Radiative Heat Transfer*, third ed., Academic Press, 2013.
- [30] M. Mohamed, M. Seaid, J. Trevelyan, O. Laghrouche, Time-independent hybrid enrichment for finite element solution of transient conduction–radiation in diffusive grey media, *J. Comput. Phys.* 251 (2013) 81–101.
- [31] M. Mohamed, M. Seaid, J. Trevelyan, O. Laghrouche, An enriched finite element model with q -refinement for radiative boundary layers in glass cooling, *J. Comput. Phys.* 258 (2014) 718–737.
- [32] A. Pourfathi, R. Tavakoli, Thermal optimization of secondary cooling systems in the continuous steel casting process, *Int. J. Therm. Sci.* 183 (2023) 107860.
- [33] J.C. Ragusa, Application of h -, p -, and hp -mesh adaptation techniques to the SP_N equations, *Transport Theory Statist. Phys.* 39 (2–4) (2010) 234–254, <http://dx.doi.org/10.1080/00411450.2010.533743>.
- [34] B. Razmjooei, A. Ravangard, L. Momayez, M. Ferchichi, The influence of heat transfer due to radiation heat transfer from a combustion chamber, *J. Therm. Anal. Calorimetry* (2021) 1–17.
- [35] Y. Saad, *Iterative Methods for Sparse Linear Systems*, PWS Publishing Company, 1996.
- [36] E. Schneider, M. Seaid, J. Janicka, A. Klar, Validation of simplified PN models for radiative transfer in combustion systems, *Commun. Numer. Methods. Eng.* 24 (2) (2008) 85–96.
- [37] M. Seaid, An Eulerian-Lagrangian method for coupled parabolic-hyperbolic equations, *Appl. Numer. Math.* 59 (3–4) (2009) 754–768.
- [38] M. Seaid, M. Frank, A. Klar, R. Pinnau, G. Thömmes, Efficient numerical methods for radiation in gas turbines, *J. Comput. Appl. Math.* 170 (2004) 217–239.
- [39] M. Seaid, A. Klar, R. Pinnau, Numerical solvers for radiation and conduction in high temperature gas flows, *Flow Turbul. Combust.* 75 (2005) 173–190.
- [40] I. Teleaga, M. Seaid, Simplified radiative models for low-mach number reactive flows, *Appl. Math. Model.* 32 (6) (2008) 971–991.
- [41] I. Teleaga, M. Seaid, I. Gasser, A. Klar, J. Struckmeier, Radiation models for thermal flows at low mach number, *J. Comput. Phys.* 215 (2) (2006) 506–525.
- [42] S. Thynell, Discrete-ordinates method in radiative heat transfer, *Internat. J. Engrg. Sci.* 36 (12) (1998) 1651–1675.
- [43] A. Vidal-Ferràndiz, A. Carreño, D. Ginestar, G. Verdú, A block arnoldi method for the SPN equations, *Int. J. Comput. Math.* 97 (1–2) (2020) 341–357.
- [44] R. Viskanta, *Radiative Transfer in Combustion Systems: Fundamental and Applications*, Begell House Publishers, 2005.